Compaction fabrics of pelites: experimental consolidation of kaolinite and implications for analysis of strain in slate

DAVID W. BAKER

Paine Gulch, Monarch, MT 59463, U.S.A.

KANWARJIT S. CHAWLA

120 Sunder Nagar, New Delhi 110 003, India

and

RAYMOND J. KRIZEK

Department of Civil Engineering, Northwestern University, Evanston, IL 60201, U.S.A.

Abstract—Compaction of clay and shale results in large reductions in volume as pore water is expelled. Preferred orientation of the platy minerals increases with compaction strain and loss of porosity according to the March–Owens model. This relationship has been studied quantitatively by experimentally consolidating kaolinite clay from slurries and analyzing the resulting fabrics with the X-ray pole figure goniometer and scanning electron microscope (SEM). 'Initial' porosity corresponds to the onset of the strain recorded by the preferred orientation; and the values of 0.78 for dispersed slurries and 0.76 for flocculated slurries reflect the electrostatic forces between the clay platelets. 'Initial' porosities of recently deposited fine silt and clay are in the range of 0.60–0.90 and are a function of grain size and mineralogy. Loss of this 'initial' porosity has a large effect on the subsequent development of slaty cleavage. Matrix methods were used to model deformation paths for slates in the Welsh slate belt. Preferred orientation of mica and ellipsoidal shapes of 'reduction' spots were simulated for one locality by loss of a 0.60 'initial' porosity, a 6° tilt of the beds and horizontal shortening involving plane strain. Strain determinations for shales and slates should include the large reduction in volume.

INTRODUCTION

PREFERRED orientation of platy minerals in pelitic rocks has proven to be a useful quantitative measure of strain in a wide variety of tectonic environments (Oertel 1983). However, determination of tectonic strain from fabric diagrams (pole figures) requires knowledge, or at least a reliable estimate, of the primary sedimentary fabric, generated during pretectonic compaction. It is the quantitative description of this primary sedimentary fabric which develops during progressive burial of clay-rich sediments, that is the subject of the experimental study in this paper. The effects of compaction fabrics on physical properties and on the development of tectonite fabrics are discussed in following sections.

Direct evidence for compaction of pelitic rocks is found in depth profiles for porosity (Rieke & Chilingarian 1974), seismic velocity (Faust 1951, Magara 1978, pp. 13–16, Hamilton & Bachman 1982), seismic velocity anisotropy (Bachman 1979, Jones & Wang 1981), and observations of microstructures using the scanning electron microscope (SEM) and the transmission electron microscope (TEM) (Bennett *et al.* 1991). Although there is considerable complexity in the manner in which porosity is lost (cf. Meade 1966, Rieke & Chilingarian 1974, Bennett *et al.* 1991), a systematic trend is observed in deep wells with hydrostatic pressure. With increasing depth, porosity decreases and seismic velocity and seismic velocity anisotropy increase as the clay platelets become increasingly aligned parallel to bedding.

EXPERIMENTAL CONSOLIDATION OF KAOLINITE

The geological process of compaction has been investigated experimentally at Northwestern University by consolidating *slurries* of kaolinite clay particles, using equipment and procedures described by Sheeran & Krizek (1971), Chawla (1973) and Edil (1973). Consolidation tests of clay samples are common in soil mechanics investigations (Yong & Warkentin 1975, Chap. 7). The studies of kaolinite consolidation by Martin (1965, 1966), Morgenstern & Tchalenko (1967), McConnachie (1974), Martin & Ladd (1975) and Griffiths & Joshi (1990), and studies of montmorillonite compaction by Bennett *et al.* (1981), are representative of the sizeable literature from other laboratories relevant to our experiments. However, lacking in these studies are quantitative analyses of fabric development in a form useful for the structural geologist. Previous studies at Northwestern University used the scanning electron microscope (SEM), the petrographic microscope and the X-ray pole figure goniometer to describe the fabrics that

Table 1. Characteristics of samples tested[*]

Parameter	Sample							
	DA-2	DA-17	FA-2	FA-17	DI-2	DI-17	FI-2	FI-17
Initial water content, w_i (%)	249	260	251	253	248	249	261	271
Final water content, w_f (%)	53	43	58	48	48	41	64	46
Final porosity, n_f	0.58	0.53	0.61	0.56	0.56	0.52	0.63	0.55
Pole density, Q_0 ($\alpha = 0°$)	3.8	4.3	2.8	3.3	1.9	0.5	2.0	0.5
Pole density, Q_{90} ($\alpha = 90°$)	0.4	0.3	0.6	0.5	0.8	1.3	0.7	1.4
Photometric intensity ratio, R	1.46	1.10	1.87	1.48	1.22	1.27	1.52	1.20
Concentration parameter, k	2.4	2.8	1.7	2.0	0.9	−1.2	1.1	−1.6
'Initial' porosity, n_i	0.78	0.78	0.76	0.76				

[*]Water content is defined as the weight of water divided by the weight of dry solids in a sample, expressed as a percentage. Porosity is the volume fraction of (water-filled) void space. Other parameters are defined and explained in the text.

develop during consolidation of kaolinite slurries (Krizek *et al.* 1975, 1977, Abdelhamid & Krizek 1976, Edil & Krizek 1976). In this paper we examine the quantitative development of preferred orientation as a function of compaction strain and the geological implications of this relationship.

Sample preparation

The stress–strain path and the pore water chemistry are the two most important factors influencing clay fabric during experimental consolidation. The samples in this study were prepared by consolidating slurries with a known chemistry under controlled stress conditions, while monitoring displacement and strain. Hydrite 10, a kaolinite marketed by the Georgia Kaolin Company, was chosen because of its particle size distribution, its well developed grain morphology, and the nature of its exchangeable ions (Krizek *et al.* 1975). Less than 5% (by weight) of the particles are larger than 2μm and less than 10% are smaller than 0.2μm. Disk-shaped platelets 1.5 μm in diameter and 0.15 μm thick are representative. Appropriate concentrations (Edil 1973) of $CaCl_2$ and NaOH were added to obtain flocculated and dispersed slurries, respectively, and these slurries were consolidated under either anisotropic stress (Sheeran & Krizek 1971) or isotropic stress (Edil 1973, Krizek *et al.* 1975) conditions to obtain bulk samples. The anisotropic stress consolidation tests were performed in a custom-fabricated consolidometer—a piston and cylinder apparatus that allows water to escape through porous stones in the piston and in the base of the cylinder, but does not allow lateral strain (Sheeran & Krizek 1971, Abdelhamid & Krizek 1976). To consolidate slurries under isotropic stress, hydrostatic pressure, applied to a spherical balloon containing the slurry, caused drainage out of two diametrically opposite ports (Edil & Krizek 1977).

The experimental design consisted of varying three parameters; namely, stress symmetry, stress magnitude and particle association in the slurry. By using two values or conditions for each parameter, there was a total of eight combinations and eight experiments (Table 1). (Edil & Krizek (1976) describe additional experiments in this series; but since both the conditions and the resulting fabrics are intermediate to those listed

in Table 1, they will not be discussed further.) The notation used to describe the samples is as follows: D = dispersed slurry; F = flocculated slurry; A = consolidation under anisotropic stress; I = consolidation under isotropic stress; and 2 or 17 represent the approximate maximum effective consolidation stresses in kg cm^{-2}. These effective stresses correspond to depths in marine clays of approximately 25 and 200 m below the sea floor (Bennett *et al.* 1977, Bryant *et al.* 1981).
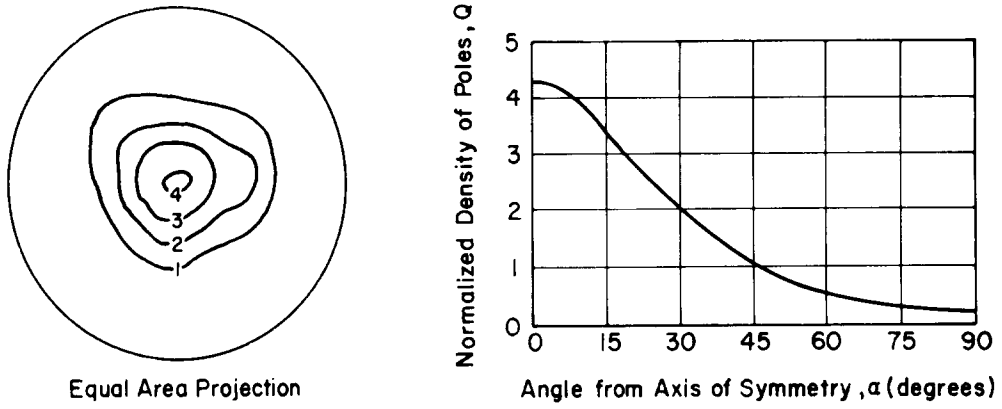
FABRIC DESCRIPTION

The X-ray pole figure, SEM micrographs and optical micrographs for sample DA-17 are shown in Fig. 1 (cf. Chawla 1973, pp. 74–75). The SEM micrograph of the horizontal plane (i.e. the plane perpendicular to the compression axis) shows a preponderance of particle faces with only a few edges, whereas the SEM micrograph of the vertical plane indicates a predominance of particle edges with definite preferred alignment in the horizontal direction. The thin section of the horizontal plane exhibits a uniform grayness as the microscope stage is rotated (as can be seen in the two optical micrographs in Fig. 1 taken 45° apart). This is because the symmetry axis of the fabric in the specimen is parallel to the axis of the microscope stage. The thin section of the vertical plane shows a uniform grayness in extinction positions, but is illuminated when the microscope stage is rotated 45°. The light intensity in these two positions was measured with a photometer, and the illumination/extinction ratio, R, listed in Table 1. In the illumination position, domains on the order of 10–20 μm in diameter can be observed. These domains can also be seen in the SEM micrograph. The maximum density of poles in the pole figure for sample DA-17 is about 4.3 times the density for an equivalent random sample (Fig. 1). Information from all three techniques shows that this sample has a strong preferred orientation of clay platelets in the horizontal plane, normal to the vertical compression axis.

Krizek *et al.* (1975) show data similar to Fig. 1 for all eight experiments. The numerical data are summarized in Table 1 (cf. Chawla 1973, p. 136). Pole figures for all eight specimens show, within experimental bounds, axial symmetry.

Fabric Reference Axis $(\alpha = 0)$: Direction of Major Principal Consolidation Stress

Equal Area Projection

Normalized Density of Poles, Q

Angle from Axis of Symmetry, α (degrees)

X-ray Diffraction Results

| Plane Normal to Fabric Reference Axis | | Plane Parallel to Fabric Reference Axis |

|←— 10 μ —→| |←— 10 μ —→|

Scanning Electron Micrographs

|←— 200 μ —→| |←— 200 μ —→|

Extinction   Illumination   Extinction   Illumination

Optical Micrographs
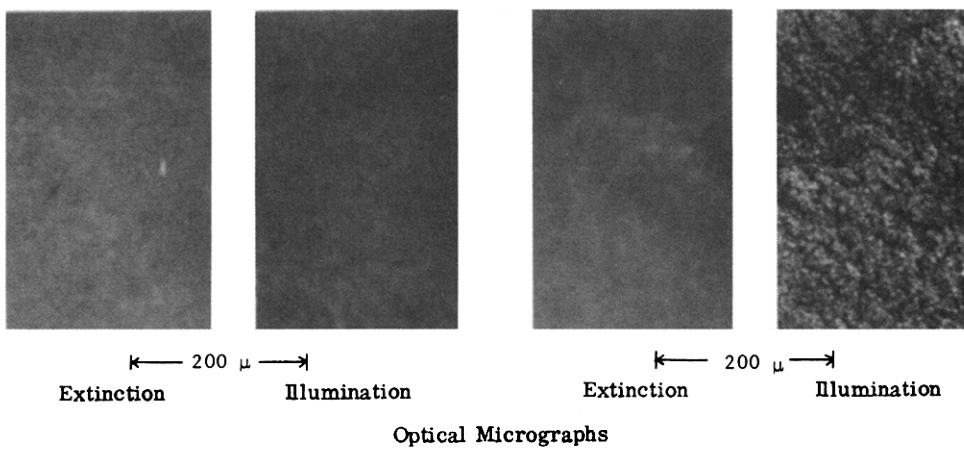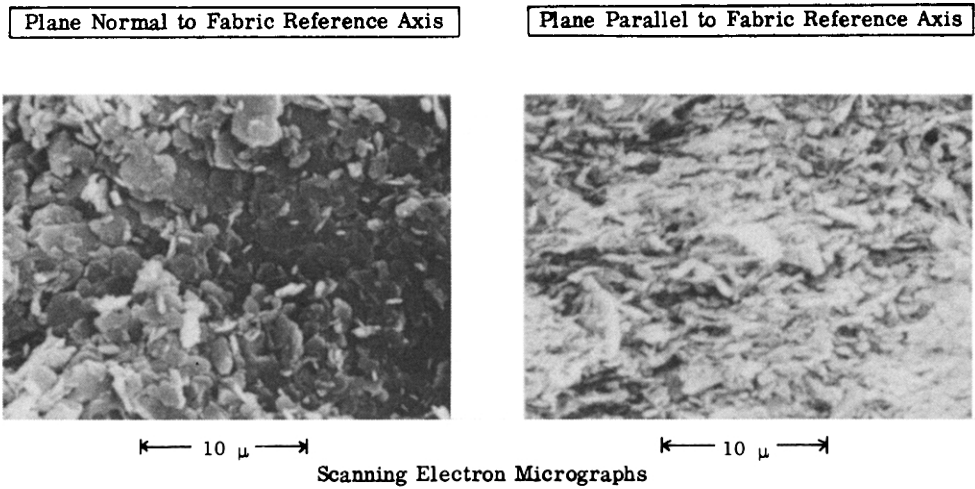
Fig. 1. Fabric description of sample DA-17.

In samples which were consolidated under anisotropic stress the symmetry axis is the piston axis. This is the direction of maximum compressive stress and greatest shortening. It is also the direction of maximum pole density.

Samples consolidated under isotropic (hydrostatic stress) have weak, but definite preferred orientation. The axis of symmetry is the general direction of drainage. In samples DI-2 and FI-2 the maximum pole density is parallel to the drainage direction, whereas in samples DI-17 and FI-17 the maximum is perpendicular to this direction forming a weak girdle pattern. These samples provide direct evidence that the development of preferred orientation of clay platelets correlates with strain, not stress. The poles to the clay platelets rotated towards the direction of greatest shortening, which at lower pressures was the axis containing the drainage ports. At higher pressures radial constriction must have exceeded axial shortening. Tullis (1971, 1976), in a fabric study of experimentally deformed mica aggregates using the X-ray pole figure goniometer, also found that preferred orientation correlated with strain, not stress.

Ideal distributions in axially symmetric pole figures

Because of axial symmetry, the pole figures can be reduced to profiles of pole density, Q, vs α, where α is the angle between a pole and the axis of symmetry. (Both the pole figures and the profiles are normalized to

multiples of the density in a uniform distribution or 'times random'.) There are two families of ideal distributions suitable for representing the pole figures and pole density profiles; namely, 'normal' distributions for non-polar lines, and pole figures derived from strain ellipsoids. Pole density profiles for samples DA-17, FA-2 and FI-2 are compared with 'normal' distributions in Fig. 2(a). Watson (1965, 1966, 1983) introduced the function $\exp(k \cos^2 \alpha)$ for poles to planes distributed with axial symmetry about a single maximum, where k is the concentration parameter (cf. Mardia 1972, p. 233). This distribution is normalized to multiples of a uniform distribution by dividing by the mean density on the reference sphere. After simplification, the expression for Q can be written as

$$Q(\alpha) = \frac{\exp(k \cos^2 \alpha)}{\int_0^{\pi/2} \exp(k \cos^2 \alpha) \sin \alpha \, d\alpha}. \tag{1}$$

The integration in equation (1) was done numerically using Simpson's rule. The agreement between theoretical and observed profile shapes shown in Fig. 2(a) is quite good, with the exception of sample FA-2, in which case the small discrepancies are attributed to experimental errors in combining data from several scans to construct a complete pole figure. With 'normal' distributions of this type only one parameter is needed to specify both the profile and the pole figure. Either the concentration parameter, k, or the pole density, Q_0, in
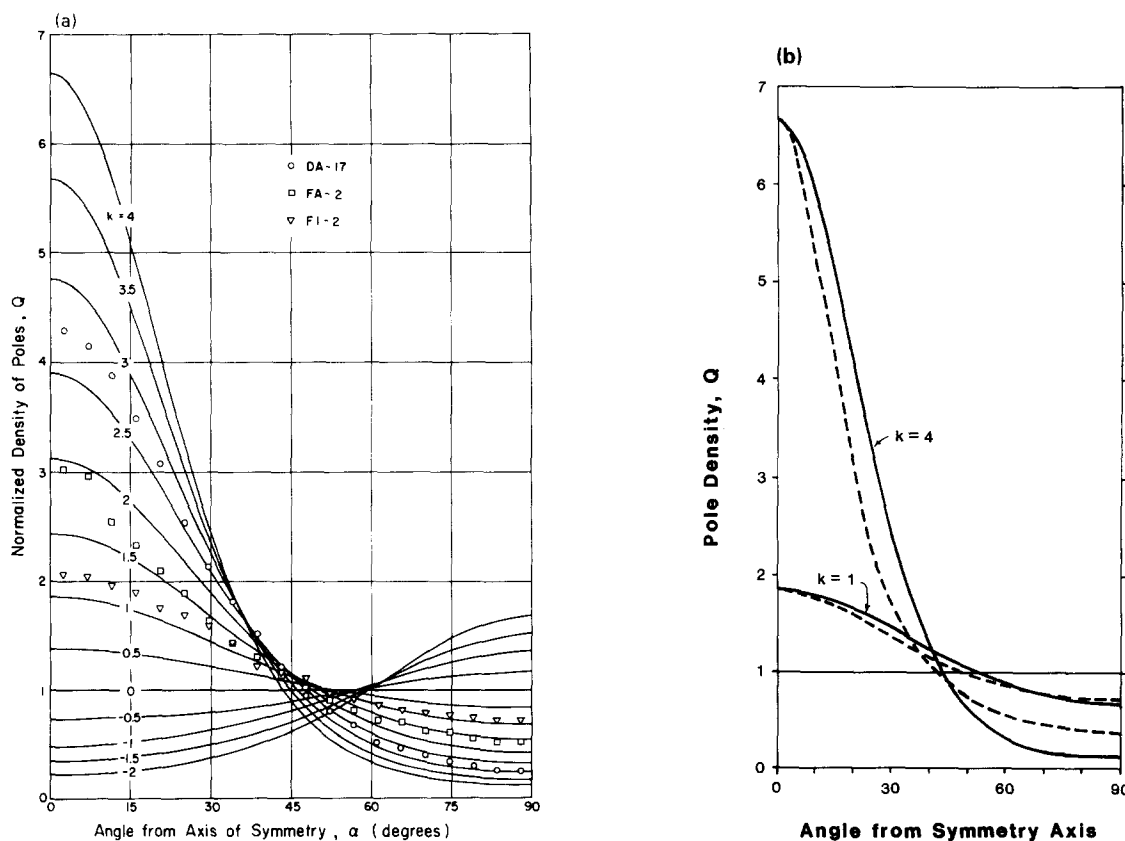

Fig. 2. Ideal distributions in axially symmetric pole figures. (a) Comparison of experimental pole density profiles with profiles through 'normal' distributions of the type $\exp(k \cos^2 \alpha)$ for 13 values of the concentration parameter, k. Symbols indicate results from three experiments. (b) Comparison of 'normal' distributions from equation (1) (solid curves) with profiles derived from strain ellipsoids using equation (4) (dashed curves), for two concentrations, $k = 1$ and 4.
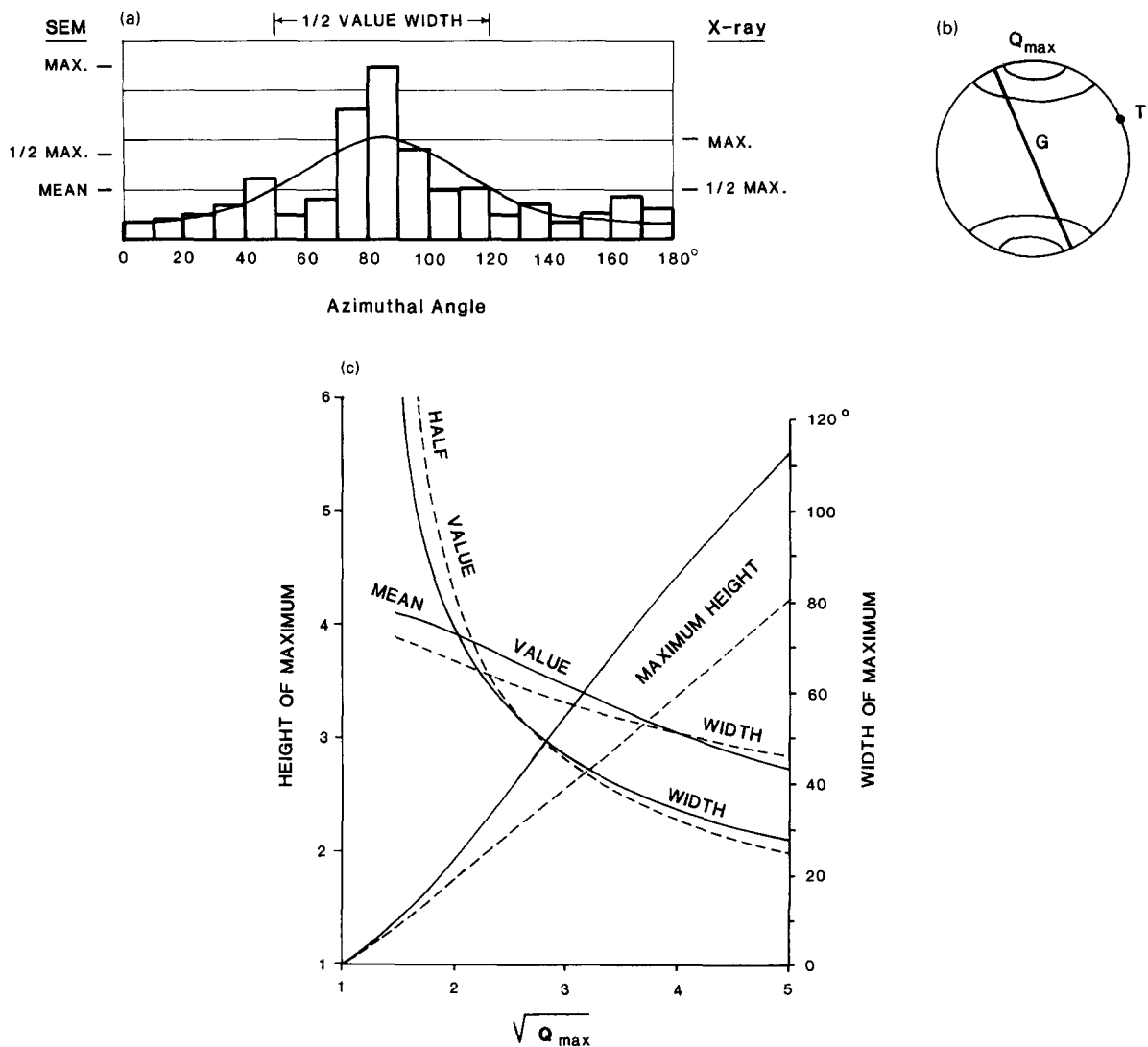
Fig. 3. Estimation of preferred orientation (Q_{max}) from SEM micrograph of section parallel to vertical symmetry axis (= short dimension of right micrograph in Fig. 1). (a) Histogram of orientations of apparent long axes of 301 grains. Azimuthal angle of long axis measured clockwise from vertical. Each orientation weighted by area of ellipse. Horizontal lines show multiples of mean. 'Bell' curve calculated from X-ray pole density profile in Fig. 1 by determining mean along great circles as shown in (b) and normalizing. Half-value width refers to 'bell' curve. (b) Equal-area projection showing orientation of poles to platelets whose apparent long axes have orientation T (= intersection of trace of plane and primitive circle). The primitive circle represents the plane of the SEM micrograph. (c) Normalized maximum value, half-value width and mean value width as a function of $(Q_{max})^{1/2}$. Solid curves—'normal' distribution. Dashed curves—distribution from strain ellipsoid.

the direction of the axis of symmetry (that is, $a = 0°$) may be used, and values for both parameters for the eight samples are listed in Table 1. If Q_0 is the maximum value in the pole figure, as is the case in all but two samples, this value will be referred to as Q_{max}.

Another ideal distribution for pole density can be derived from the strain ellipsoid using the March model (dashed curves in Fig. 2b). The formula for this distribution is given in a later section. This distribution can also be characterized by a single parameter. The experimentally determined profiles as plotted in Fig. 2(a) do not coincide with curves for this distribution. However, Oertel (1983, pp. 418–419) discussed the practical difficulties in determining the background value for a diffraction peak scanned with the X-ray pole figure goniometer. By suitable changes in background values the experimental profiles can be made to nearly coincide with curves generated from strain ellipsoids.

Estimating Q_{max} from SEM micrographs

Because only one value is needed to completely specify either of the ideal distributions, the effect of changing conditions, such as strain or pore fluid chemistry, on preferred orientation is easily portrayed. It is useful to estimate the value of Q_{max} from SEM micrographs to compare with X-ray determinations.

Disk-shaped platelets inclined to the plane of a SEM micrograph appear as ellipses. The orientation in the micrograph of the long axis of each ellipse is easily measured with a protractor, and the length of the long and short axes, with a ruler. The orientations, weighted by the area of each ellipse can be plotted in a histogram or rose diagram. Figure 3(a) shows the histogram of the orientation of the longest dimension of grains in the SEM micrograph on the right side of Fig. 1. The mean value line is the total area of grains counted, divided by

the number of cells used (18). Three readily determined parameters characterize the histogram, namely; (1) the height of the maximum, expressed as a multiple of the mean value; (2) the width of the peak (in degrees) measured at positions which are half the peak height; and (3) the width of the peak at the mean value.

To construct graphs showing the values of these three parameters as a function of Q_{max} takes several steps. In Fig. 3(b) the poles to all platelets, whose apparent long axes have the orientation, T, lie along the great circle, G, normal to T. The density of long axes at T is the mean pole density along G. By letting T assume successive positions along the primitive circle, one can construct a frequency profile. Such a profile, normalized by the mean value of the profile, is shown in Fig. 3(a) for sample DA-17. Figure 3(c) shows how normalized peak height and the peak widths vary with the degree of preferred orientation for both ideal distributions.

Using the curves in Fig. 3(c), the histogram in Fig. 3(a) can be used to estimate the preferred orientation in sample DA-17, but several factors limit the accuracy of the estimate. The histogram in Fig. 3(a) is weakly bimodal. The secondary peak at an azimuth of 45° corresponds to thin zones of aligned grains, indicating incipient development of a secondary spaced cleavage. Diagonal boundaries between domains are visible both in thin section and SEM micrographs (cf. Krizek et al. 1975). A second factor is operator bias. The long axes of the grains in this highly oriented specimen were drawn on a sheet of tracing paper by inspection. Visual perception of grains in the micrograph emphasizes their parallelism and the histogram shows a greatly sharpened central peak compared with the profile generated from the 'normal' distribution ($Q_{max} = 4.3X$). The technique of Erslev & Ge (1990) to reduce operator bias is to locate at least five points along the margin of each grain and use the method of least squares to determine the best fitting ellipse. A digitizing tablet attached as a peripheral device to a personal computer makes such an approach practical.

INTERPRETATION OF FABRICS

From quantitative data listed in Table 1 for the eight samples tested, it can be seen that there are systematic differences in behavior. Samples consolidated from dispersed slurries are slightly more compressible than those consolidated from flocculated slurries; that is, they have a lower porosity for a given state of stress. In the anisotropically consolidated samples the degree of preferred orientation, as measured by k or Q_{max}, increases with increasing axial strain; however, for a given axial strain or porosity the preferred orientation is greater in the dispersed samples than in the flocculated ones (Fig. 4). The negative values of k in Table 1 for the two samples consolidated in the spherical balloon under a high hydrostatic consolidation stress (17 kg cm^{-2}) indicate girdle, rather than single maximum, fabrics.

Morgenstern & Tchalenko (1967) suggested that the

photometric intensity ratio could be used for fabric analysis of petrographic thin sections of experimentally consolidated kaolinite. However, as shown in Fig. 4, R drops sharply as porosity is lost. Light traveling through the thin section passes through many overlapping grains with inclined grain boundaries where it is refracted and reflected. The resulting scattering and depolarization render this technique unsuitable for quantitative analysis.

Compressibility and degree of preferred orientation

In a flocculated slurry, the net forces between particles are conducive to the formation of edge-to-face contacts, whereas in a dispersed slurry the net interparticle force regime tends to favor the formation of face-to-face contacts. If the net forces between particles are smaller, as in the case of a dispersed slurry, the particles are freer to move past one another, thereby leading to greater deformation for a given state of stress. Since most of the negative charge on a clay platelet resides on the faces rather than on the edges, the platelets in a dispersed slurry tend to be aligned in a parallel fashion, and this arrangement gives the maximum spacing between the faces of adjacent platelets. Accordingly, the tendency of platelets to orient themselves normal to the direction of greatest shortening is enhanced by rotations due to the electrostatic forces between particles, thus leading to stronger preferred orientation in dispersed samples.

Quantitative model for development of preferred orientation during anisotropic consolidation

Platelet-shaped particles embedded in a deforming viscous medium rotate towards the plane of greatest flattening in the local strain field. March (1932) derived an expression that gives the pole density, Q, of the platelets as a function of strain, assuming that the platelets are randomly oriented before the onset of any deformation. Owens (1973) extended the March analy-
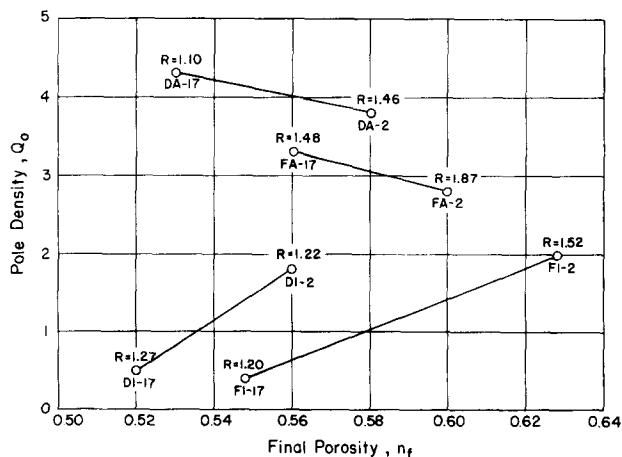

Fig. 4. Preferred orientation of experimentally consolidated kaolinite as a function of final porosity. R—photometric intensity ratio (illumination/extinction).

sis to include the effects of changes in volume and any initial distribution of pole densities. His general relationship is

$$Q_f = \frac{V_f}{V_i}\left(\frac{l_i}{l_f}\right)^3 Q_i = \frac{V_f}{V_i}(1 + \varepsilon)^{-3}Q_i, \qquad (2)$$

where Q is the density of poles parallel to a line whose length is l, ε is the elongation of the line, the stretch of the line, $l_f/l_i = (1 + \varepsilon)$, V is the volume, and the subscripts i and f refer to initial and final conditions, before and after the deformation, respectively (cf. Tullis 1971, p. 195). Porosities (n_i, n_f) are the volume fractions of void space. Hence $(1 - n)$ is the volume friction of particles. The volume ratio in (2) can therefore be expressed in terms of porosities as

$$\frac{V_f}{V_i} = \frac{1 - n_i}{1 - n_f}. \qquad (3)$$

If X, Y and Z are the principal stretches, i.e. axes of the strain ellipsoid (cf. Ramsay 1967, pp. 121–166), then for an initially random fabric, $Q_x Q_y Q_z = 1$ and $XYZ = V_f/V_i$.

'Ideal' distributions or pole figures can be generated from the (inverse of the transpose of the) strain ellipsoid matrix using equation (2) and the equation for the length of a line in any direction (Nye 1957, p. 26, equation 33, Ramsay 1967, equation 4-5). (For matrix equations, cf. Owens 1973, p. 251, Flinn 1978, equation 26, Wheeler 1986, equation 4.) To generate the contour lines in a pole figure, one selects the stretch that corresponds to a particular contour level, e.g. $2X$. Ramsay's equation (4–5) then becomes an equation for one direction cosine in terms of another (cf. Ramsay & Huber 1983, p. 205, equation 11.18). Two direction cosines, of course, are sufficient to locate a pole in the pole figure, using the equations for equal-area projection. By varying the one direction cosine in small increments, and calculating the second direction cosine, one can draw the contour line as a series of short straight line segments—a technique well suited for programming on a personal computer.

In the case of uniaxial consolidation in which the axes of the strain ellipsoid are $X = Y = 1$, $Z < 1$, and the volume ratio in equation (3) is Z, the expression for pole density profiles can be derived from equation (2) as

$$Q = \frac{Z}{[Z^2 + \sin^2 \alpha\,(1 - Z^2)]^{3/2}}. \qquad (4)$$

In comparison with the profiles for 'normal' distributions given by equation (1), the peaks from equation (4) are narrower and sharper, and the minimum value is closer to unity (Fig. 2b). This distribution has the convenient property that $Q_{max}(Q_{min})^2 = 1$.

The maximum preferred orientation that develops due to vertical uniaxial strain in the consolidometer can be expressed by a simplified version of equation (2) (Oertel & Curtis 1972, Chawla 1973). Thus,

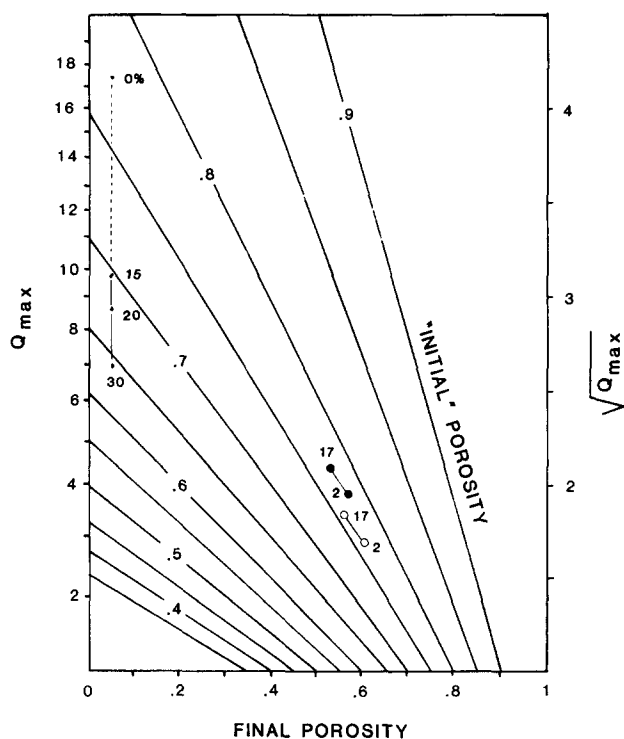$$Q_{max} = \frac{1}{(1 + \varepsilon)^2} = \frac{1}{Z^2} = \left(\frac{1 - n_f}{1 - n_i}\right)^2, \qquad (5)$$

FINAL POROSITY

Fig. 5. Relationship of preferred orientation (Q_{max}), final porosity and 'initial' porosity. Solid dots—DA samples; open circles—FA samples (number gives consolidation stress). Small dots near left margin give quartz content in mudrocks of Curtis et al. (1980) and extrapolated quartz-free value.

where ε is the vertical compaction strain, n_f is the final porosity, and there is no lateral (horizontal) strain. The 'initial' porosity, n_i, is defined as the porosity when the grains first form a three-dimensional framework, which is then deformed as the consolidation continues. By taking the square root of equation (5), one can generate a family of straight lines for the square root of Q_{max} vs n_f with n_i as the parameter (Fig. 5). The data for our kaolinite experiments indicate an 'initial' porosity of 0.78 for the dispersed slurry and 0.76 for the flocculated slurry. The higher 'initial' porosity in the dispersed slurry is due to repulsive electrostatic forces between the kaolinite platelets.

Plots of void ratio, $e = n/(1 + n)$, vs log(pressure) for slurry-consolidated kaolinite show a sharp bend at values corresponding to porosities of approximately 0.62–0.69 (Morgenstern & Tchalenko 1967, Sheeran & Krizek 1971, McConnachie 1974, Martin & Ladd 1975), indicating the point at which the axial load begins to be supported by the framework of kaolinite grains, i.e. the liquid limit of the clay (cf. Abdelhamid & Krizek 1976, fig. 4). The values for 'initial' porosity of 0.76–0.78 in Fig. 5 are much higher and indicate that significant deformation is recorded by the preferred orientation before the clay slurry acquires measurable compressive strength. Thus, we picture 'initial' porosity as the point in the consolidation history at which the kaolinite platelets have come into contact with one another and their poles start rotating towards parallelism with the vertical piston axis in a statistically coherent manner. This point

corresponds to the 'fluid limit' of Monté & Krizek (1976).

Estimating strain from center-to-center plots of SEM micrographs

Although the center-to-center technique of Fry (1979) for determining strain is well established in structural geology (cf. Ramsay & Huber 1983, pp. 107–125), this simple and effective technique apparently has not been applied to the analysis of deformed clay. The technique consists of determining and displaying the distance and direction between the center points of all pairs of grains in a micrograph. The low density elliptical shaped area round the origin in Fig. 6(a) describes the 'nearest neighbor' configuration of the kaolinite platelets in sample DA-17. According to Fry's method, this ellipse has the same shape as the strain ellipse. The ratio of the short axis to the long axis of the ellipse of approximately 0.5 (= Z) and the final porosity of 0.53 can be used in equation (5) to calculate an 'initial' porosity of 0.77, which compares favorably with the value obtained using X-ray data. The strain recorded by the center-to-center technique is the compaction strain after the grains have come into contact with one another.

Fry's (1979) technique can be considered at the 'low-tech' end of the spectrum of available analytical techniques. It is easy, relatively quick and gives meaningful results. Crespi (1986) discusses practical limitations of the technique. Erslev (1988) and Erslev & Ge (1990) have made several modifications and enhancements to the technique which require more measurements (Fig. 6b). Erslev's program INSTRAIN, when used with a digitizing tablet, eases the burden of data collection and analysis.

At the other end of the spectrum are digital image processing systems and the elaborate mathematical techniques for stereological specification of anisotropy (Kanatani 1984, 1985). For example, Altschaeffl & Thevanayagam (1991) measure the configuration of pore space and estimate strain by expanding a 'fabric' tensor to only the second order. It remains to be demon-

strated whether these more elaborate techniques will provide more meaningful strain data than that obtained with Fry's (1979) simple graphical technique.

COMPACTION OF MUD AND SHALE

The techniques we used in our laboratory study can be used to analyze naturally occurring clay-rich mud and shales. The most accurate and direct method to measure preferred orientation of platy minerals in clays and shales is with transmission scans on the X-ray pole figure goniometer. TEM (and SEM) micrographs, showing the orientation of clay platelets on sections perpendicular to bedding, can also be analyzed by constructing histograms similar to Fig. 3(a) and using the graphs in Fig. 3(c) to estimate the value of Q_{max} or k. The center-to-center technique, illustrated in Fig. 6, directly measures strain in oriented sections.

Our experimental study has implications for fabrics which develop in clay-rich muds and shale during compaction. We model the compaction processes as follows. Clay particles, deposited on the sea floor, usually as floccules, have random orientations (Bennett *et al.* 1991). During compaction the clay platelets rotate towards horizontal. Their poles form a maximum which is initially very diffuse, but with increasing compaction becomes sharper. In undisturbed sediments this maximum is vertical and has axial symmetry. The ideal distribution in equation (4) describes the preferred orientation of the clay platelets, requiring only one number, either Q_{max} or Z. Preferred orientation as a result of compaction strain develops according to equation (5). The plot of the square root of Q_{max} vs final porosity covers a field in Fig. 5 with 'initial' porosity as the parameter. 'Initial' porosity, i.e. the porosity of sediments on the sea floor, is thus a critical parameter.

According to Meade (1966) the main factor controlling 'initial' porosity is grain size (and secondarily, mineralogy). Figure 7 gives the general trends in several marine environments. Mitchell (1976, fig. 4.14) indicated the variation in sorting vs median grain size in
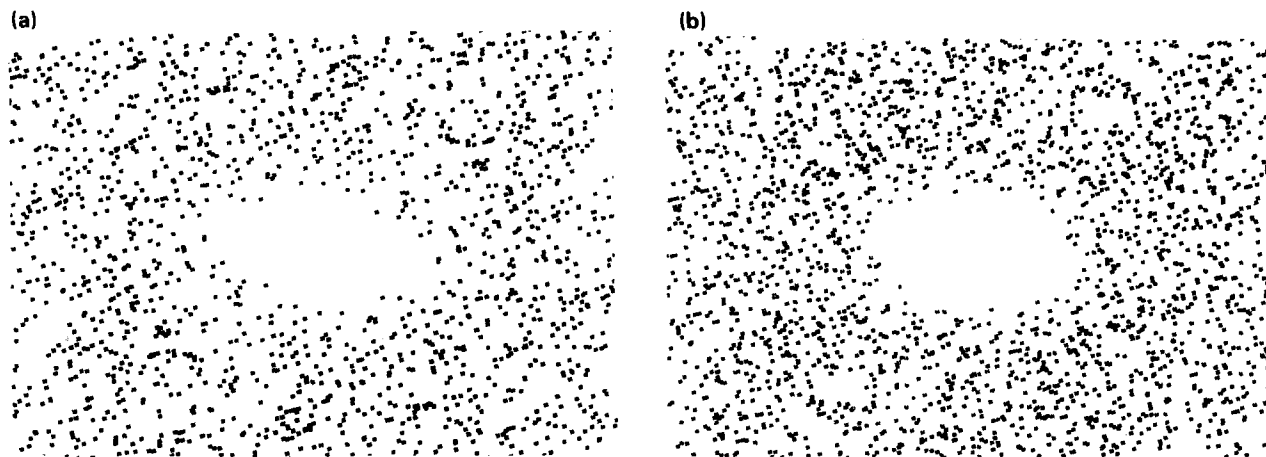
(a)

(b)

Fig. 6. Estimation of strain from SEM micrograph parallel to symmetry axis (301 grains in Fig. 1). (a) Fry's (1979) center-to-center diagram. (b) Erslev's (1988) normalized Fry diagram.
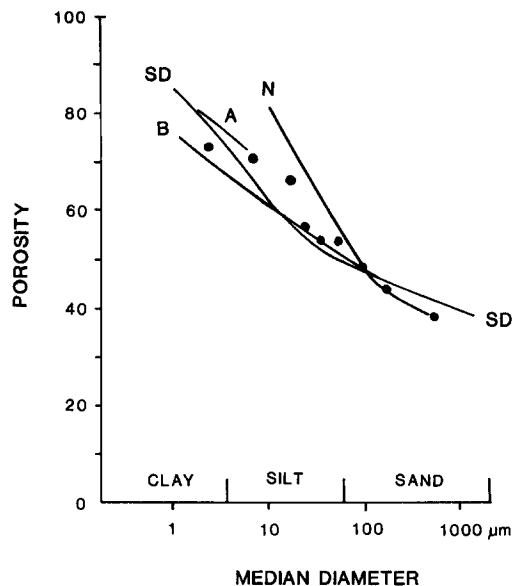
Fig. 7. 'Initial' porosity (volume %) in recent sediments as a function of median grain size. N = North Sea and SD = San Diego Bay (after Meade 1966). A = abyssal plain; dots = continental shelf and slope (after Hamilton & Bachman 1982). B = composite of DSDP data (after Bryant *et al.* 1981, fig. 30).

marine and non-marine sediments. Curtis *et al.* (1980) suggest $n_i = 0.80$ for sediments with at least 60% of <2 μm clays and $n_i = 0.60$ for silts with less than 20% of <2 μm clays. Of the three most common clay minerals, montmorillonite tends to form clays with the smallest grain size and highest 'initial' porosities, illite clays are intermediate, and kaolinite clays have the largest grains and lowest initial porosities (Bryant *et al.* 1981).

Although shale is a very common rock type, there are only a small number of studies using the X-ray pole figure goniometer (Oertel & Curtis 1972, Curtis *et al.* 1980, Schiller 1980, Feeser 1986). Curtis *et al.* (1980) determined the preferred orientation in Carboniferous-age mudrocks from southern Yorkshire in England (which fall in the siltstone grain-size classification) with final porosities of about 0.05, and found a good correlation between Q_{max} and quartz content. Their thin section micrographs indicate that this trend also reflects grain size. The extrapolation of their trend to a quartz free, i.e. all platy mineral, composition corresponds to an 'initial' porosity of 0.77, in excellent agreement with our experimental data (Fig. 5). The 'initial' porosities shown in Fig. 5 of 0.64–0.69 for the mudrocks are in the range typical for silts (Fig. 7).

Schiller (1980) used the X-ray pole figure goniometer in the reflection mode to obtain partial pole figures for 114 shale and siltstone specimens in Germany. He also determined porosity and modal composition and estimated the grain size in thin sections. His parameter for preferred orientation is the half-value width of the maximum in the pole figure, which he defined as the angle from the symmetry axis at which the pole density is the average of the maximum and minimum values. As shown in Fig. 2, this angle in 'normal' distributions does

not exceed 45°; however, Schiller listed values up to 75°. The reflection mode, in contrast to the transmission mode, requires large intensity corrections (Baker *et al.* 1969, fig. 3). After correcting Schiller's data for this effect, we used the 'normal' distributions shown in Fig. 2 and equation (5) to estimate values for 'initial' porosity. Figure 8 shows that clay mineral content and grain size are inversely correlated and that the 'initial' porosity is a function of both. The results using distributions derived from strain ellipsoids (equation 4) are similar, but the 'initial' porosities are higher. Schiller (1980) also showed that the development of preferred orientation is inhibited by the presence of carbonates, presumably due to porosity loss by cementation rather than compaction (cf. Bryant *et al.* 1981, fig. 34). Thus, we omit discussion of shales containing carbonates. On the other hand, Schiller (1980) noted that organic material is highly compressible and its presence enhances preferred orientation.

ANISOTROPY OF PHYSICAL PROPERTIES IN CLAYS AND SHALES

Preferred orientation of platy minerals in a rock causes anisotropy in many of its physical properties. Krizek *et al.* (1977) showed how the anisotropy of creep strength in the same samples used in this study results from the preferred orientation. Creep strength is an important soil mechanics parameter affecting the stability of foundations, dams and other structures as well as geologic masses subject to downslope movements.
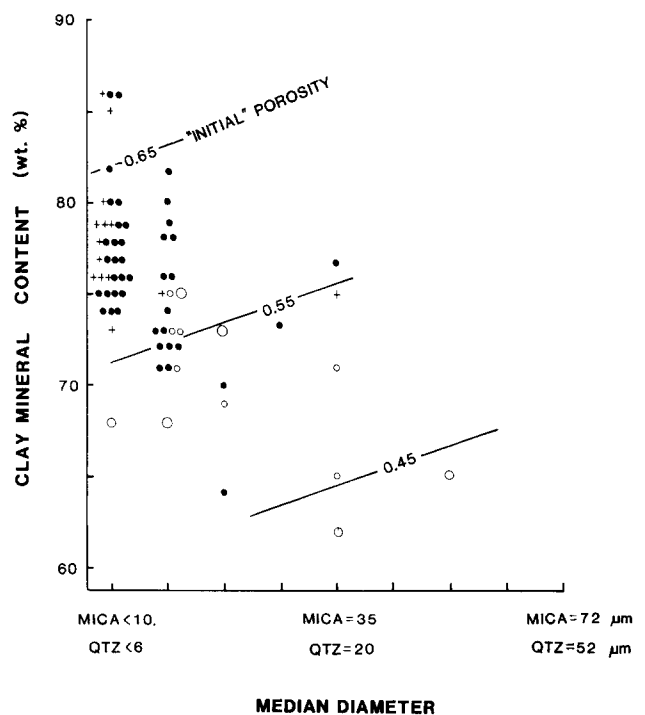

Fig. 8. Estimated 'initial' porosities in Carboniferous shale and siltstone containing less than 5% carbonate. Data adjusted from Schiller (1980) as discussed in text. Symbols for 'initial' porosities: +, >0.65; ●, 0.65–0.55; ○, 0.55–0.45; ○ <0.45. Contours based on multiple linear regression with $R_2 = 0.53$.
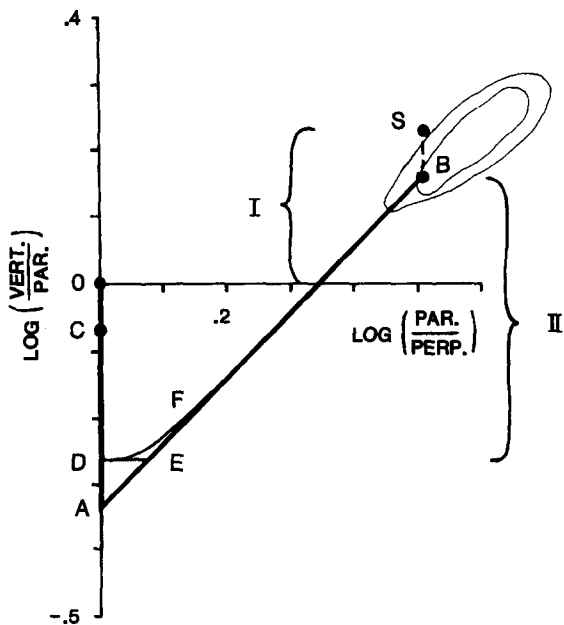
Fig. 9. Coaxial deformation plot (log Flinn diagram) for slate. Horizontal tectonic axes are parallel (par.) and perpendicular (perp.) to slate belt. Third axis is vertical (vert.). Base for logarithms = 10.

Elastic properties of shale are strongly affected by preferred orientation of platy minerals. The technique of Baker & Carter (1972) can be used to determine the five elastic constants for an aggregate with axial symmetry from single crystal constants and the preferred orientation. Given the elastic constants, the seismic velocity anisotropy can be calculated. Jones & Wang (1981) and Heard & Lin (1986) used the alternate approach for shale specimens and measured the set of five elastic constants and ultrasonic velocities as a function of pressure in the laboratory. Wood et al. (1976) determined both the sonic velocities and the mica pole figure for Welsh slate from the Penrhyn Quarry. Bachman (1979) reviewed seismic velocity anisotropy in marine sediments.

STRAIN ANALYSIS OF SLATES

Oertel (1983) reviewed studies using the X-ray pole figure goniometer to determine strain in pelitic tectonites and concluded that the technique is indeed robust and successful in a wide variety of geological situations. Because the pole densities include the effect of compaction, reliable estimates of compaction strains are needed to determine the portion of strain due to tectonic deformation. The intent here is to illustrate the effect of compaction fabric in a well-studied area with a relatively simple tectonic history and abundant quantitative data—the Welsh slate belt (Wood 1974, Tullis & Wood 1975, Wood & Oertel 1980). A thick sequence of shale was deposited there in the Late Cambrian with the slaty cleavage forming in the Late Silurian (Dalziel 1969, Dewey 1969).

In its simplest form the deformation path for these slates is vertical compaction followed by horizontal shortening (Fig. 9), whereby all strain is coaxial and

there is no change in the intermediate axis of the strain ellipsoid. Thus, the tectonic strain is plane strain. The deformation path in Fig. 9 is shown in the logarithmic deformation plot of Flinn (1978, figs. 1c & d and 4a) in which the $X \geqslant Y \geqslant Z$ convention is relaxed and tectonic axes are used. This deformation path is illustrated by Ramsay & Huber (1983, pp. 185–188) and discussed by Ramsay & Wood (1973), Sanderson (1976), Flinn (1978) and Bell (1985). It consists of deposition (O), compaction until all porosity is lost (O − A) and plane strain tectonic deformation (A − B).

Tullis & Wood (1975), Wood et al. (1976) and Wood & Oertel (1980) show pole figures for 001 of mica in slate from quarries along the Welsh slate belt. The preferred orientation of mica can be used to determine the strain ellipsoid using equation (2); however, Oertel (1983) described the practical difficulties in determining the X and Y values of the strain ellipsoid from X-ray peak intensities that are not much different from background. Figure 10 shows a grid in a logarithmic deformation plot for two parameters which are easily measured in pole figures presented as equal-area projections with the maximum pole density in the center (cf. Wood et al. 1976, fig. 3). Values for Q_{max} and the aspect ratio of the oval-shaped $2X$ contour (long diameter divided by the short diameter) allow the ratios of the strain axes to be determined. (As discussed in a previous section, pole figures can be derived from the strain ellipsoid, and the shape of the $2X$ contour and Q_{max} can be calculated as a function of the principal axes, X, Y and Z.) The value plotted in Fig. 10 is for locality 7 in Wood & Oertel (1980). This value is shown as B in Fig. 9 together with
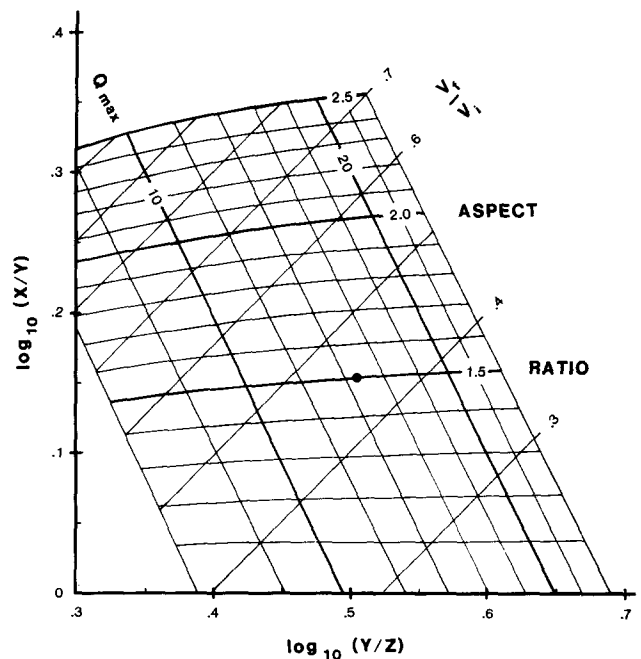

Fig. 10. Determination of strain ratios from pole figures for mica in slate. Pole figures must have a single maximum and orthorhombic symmetry. The steeply inclined contours are for Q_{max}. Sub-horizontal contours are for the aspect ratio (long axis/short axis) of the $2X$ contour. Dot—locality 7 in Wood & Oertel (1980). Contours for the volume ratio, V_f/V_i, are only valid for tectonic plane strain (cf. Ramsay & Wood 1973).

the value for the mean shape of ellipsoid-shaped 're-
duction' spots in the spotted slate (point S). The differ-
ence in strains recorded by the mica and the 'reduction'
spots at this locality can be explained if the sediment had
compacted by the amount C in Fig. 9 before a spherical
diffusion halo (point 0) formed around an object (per-
haps of organic origin). The difference (0 − C) is carried
through progressive deformation and appears as the
difference (S − B).

Also shown in Fig. 9 are the areas of highest density in
Wood's (1974, fig. 4) plot of 5200 determinations of
strain ellipsoids (the majority of which were 'reduction'
spots in Welsh slate). Ramsay & Wood (1973) showed
that, in the case of rocks which had lost volume and then
were deformed by coaxial plane strain, the deformation
path would plot along a line with a slope of unity, but
shifted to the right of the origin in the deformation plot
by an amount corresponding to the (negative) dila-
tation. The most frequent strain states measured by
Wood (1974) define a path of plane strain close to the
volume ratio contour of 0.4 in Fig. 10 or a volume loss of
0.6 (cf. Ramsay & Wood 1973, p. 274). As shown in Fig.
7, this value of 0.6 for 'initial' porosity corresponds to
silt.

According to Dalziel (1969, p. 24) there were approxi-
mately 5 km of Cambrian strata in North Wales and the
total thickness of Lower Paleozoic rocks may have
exceeded 15 km. Thus, Ramsay & Wood (1973) argued
that the amount of porosity left in the shales at the onset
of tectonic deformation did not exceed 20% and was
likely much less (cf. Rieke & Chilingarian 1974, pp. 41–
52). Two coaxial deformation paths for partially com-
pacted shales are shown in Fig. 9. Since compaction is
uniaxial strain in which the reduction in volume corre-
lates 1:1 with the vertical shortening, we consider the
same behavior continues along the path D–E when the
shortening direction changes from vertical to
horizontal—at least initially. The argument is that if the
strain rate is slow enough for the pore water to escape, it
is easier for the horizontal shortening to be accommo-
dated by volume loss in a soft sedimentary rock than by
vertical extension which lifts the overburden. Thus,
according to this model, any remaining pore water is
squeezed out of the shale during the initial stages of
tectonic deformation (cf. Bell 1985).

A second possibility, illustrated in Fig. 9, considers
that at the onset of tectonic deformation the rate of
volume loss equals the rate of horizontal shortening, but
that it decreases according to a hyperbolic curve (cf.
Flinn 1978, fig. 4d):

$$\text{volume ratio} = \frac{V_f}{V_i} + \frac{(V_c/V_i - V_f/V_i)^2}{(1 - Y) + (V_c - V_f)/V_i},$$

where the volume ratio of the solids, V_f/V_i, is $(1 - n_i)$ in
equation (2), Y is the principal axis of the strain ellipsoid
in the horizontal direction perpendicular to the slate belt
and V_c is the volume at which vertical compaction
stopped. The deformation path for this model is D–F in
Fig. 9.

The results show that for the *coaxial* strain models

shown in Fig. 9 the resulting strain is independent of
path and the most important parameter is 'initial' poro-
sity. Porosity is lost and then the deformation proceeds
along the diagonal path of plane strain.

Of course, coaxial strain is an unrealistic simplifi-
cation. General strain, however, leads to an unlimited
number of possible deformation paths. Two families of
'simple' deformation paths, which are perturbations to
the plane strain path in Fig. 9, have sufficient degrees of
freedom to allow matching of observed data by varying a
small number of parameters. One family is generated by
gently tilting the beds after compaction, but before
tectonic deformation (cf. Oertel 1970, Tullis & Wood
1975, Bell 1985). The other family is generated by
allowing small amounts of shear strain due to differential
horizontal shortening to occur in addition to the domi-
nant pure shear (cf. Ramsay & Wood 1973, fig. 9, Wood
1974, figs. 6–8).

We used the matrix method of Flinn (1978) to investi-
gate the first family of deformation paths. The path of
progressive deformation in the deformation plot can be
generated by calculating the strains and strain ellipsoids
resulting from a series of incremental deformations (cf.
Ramsay 1967, pp. 326–332), but an equal-area projec-
tion is needed to follow the dramatic reorientation of the
principal strain axes with respect to the tectonic axes (or
vice versa). Figure 11 shows a simulation which matches
the data measured by Wood & Oertel (1980) at their
locality 7. The path is similar to 0–D–E–B in Fig. 9.
However, at point D the beds were gently tilted.

A detailed description of the model in Fig. 11 is as
follows. The clastic deposit destined to become slate was
deposited as silt with an 'initial' porosity of 0.6. 'Re-
duction' spots formed after loss of 0.11 of the volume
(point C). Burial and compaction continued until pore
water that had occupied 0.55 of the original volume was
expelled (point D). Then the beds were tilted 6° about a
horizontal axis trending 70° from the slate belt. The co-
ordinates in Fig. 11(b) are axes of the strain ellipsoid and
the 6° tilt is shown by the small jump of the vertical
direction from the center of the projection towards the
'P' in 'Perpendicular'. Uniaxial horizontal shortening
expelled the remaining pore water (D–E in Fig. 11a).

All subsequent deformation was constant-volume
plane strain (pure shear) with horizontal shortening and
vertical extension. The fractional shortening in the
direction perpendicular to the slate belt at each incre-
ment was 0.05. Due to the tilt of the beds the incremen-
tal strain ellipsoid and the total strain ellipsoid were not
coaxial. After each increment the orientations and mag-
nitudes of the axes of the total strain ellipsoid were
calculated as eigenvalues of the total strain tensor. The
values used in the deformation plot in Fig. 11(a) are
principal axes of the strain ellipsoid closest to the tec-
tonic directions of 'vertical', 'parallel' and 'perpendicu-
lar'. When the X axis of the total strain ellipsoid was
subparallel to the 'parallel' tectonic axis, the defor-
mation path (heavy curve in Fig. 11a) followed the thin
straight line for plane strain, but the path diverged from
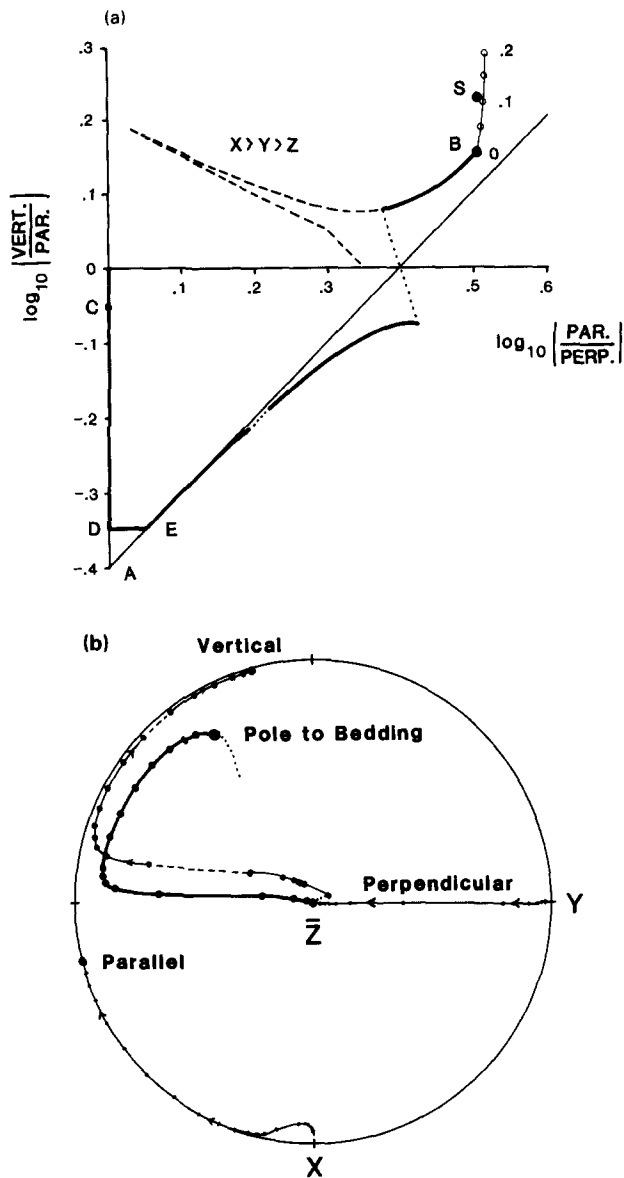this line as the difference in orientation increased. At E

Fig. 11. Simulation of Welsh slate—locality 7 of Wood & Oertel (1980, fig. 7). (a) Deformation plot (cf. Fig. 9). (b) Equal-area projection on lower hemisphere of pole to bedding and tectonic axes, vertical, parallel, perpendicular, with respect to strain axes, X, Y and Z. Z = pole to cleavage. X = lineation.

the shortest axis of the total strain ellipsoid, Z, was subvertical, but with progressive deformation the strain axis closest to vertical became Y and then X. The short gap with dots in the deformation path in Fig. 11(a) indicates the switch from Z to Y. The long gap with dots which crosses the abscissa is the jump from Y to X. Of course, the strain ellipsoid changed its orientation in a continuous manner and the 'jumps' are merely an artifact of the convention for the deformation plot that uses the strain axis closest to a tectonic axis. The orientations of the vertical axis corresponding to 'jumps' in the deformation plot are shown by dashes in Fig. 11(b).

For comparison, the same deformation path is shown in conventional format by the dashed line labeled '$X > Y > Z$' in Fig. 11(a), using $\log_{10}(X/Y)$ as the ordinate and $\log_{10}(Y/Z)$ as the abscissa. An abrupt reversal in direction rather than a 'jump' indicates a switch in axes. Bell

(1985) gives an extensive discussion of this form of the deformation plot.

The term 'dramatic reorientation' used in a previous paragraph also refers to the path for the pole to bedding in Fig. 11(b), which was parallel to the compaction direction, $-Z$, but rotated first towards $-Y$, then towards the lineation, $-X$. The large black dot shows the orientation of bedding observed by Wood & Oertel (1980, fig. 6). Had the horizontal shortening continued, the pole to bedding would have rotated towards the pole to cleavage, $-Z$, as indicated by the trail of small dots in Fig. 11(b), thus completing a large loop.

The small open circles on the curve extending up from B in Fig. 11(a) show the axial ratios of 'reduction' spots which formed after the sediment had compacted for fractional amounts ranging from 0 to 0.2. This is the basis for the estimate that the observed axial ratios, shown as S, correspond to a fractional volume loss of 0.11 before the diffusion halos formed.

The model in Fig. 11 was able to simulate both the interrelationships of bedding, cleavage, lineation, Q_{max} and aspect ratios, and the axial ratios of the 'reduction' spots for locality 7. However, a small post-tectonic tilt is required to bring bedding, cleavage and lineation to the attitudes observed in the slate quarry. Similar deformation paths involving compaction, gentle tilting, and plane strain are able to simulate the relationships among bedding, cleavage, lineation and strain ellipsoid, at other localities described by Wood & Oertel (1980). However, attempts simultaneously to match the observed axial ratios of the 'reduction' spots using this simple model were unsuccessful. Investigation of the second family of 'simple' non-coaxial deformation paths offers possibilities, but is a topic for future research.

As demonstrated in Fig. 11 'lost' porosity has a large effect on the development of slaty cleavage. In our simulation, the principal stretches or axes of the strain ellipsoid, X, Y and Z, for the successful match to observed data are:

Constant volume strain ellipsoid
[1.87, 1.31, 0.41].

Total strain ellipsoid ($V_f/V_i = 0.40$)
[1.37, 0.97, 0.30].

Compaction strain ellipsoid
[1, 1, 0.4].

Tectonic strain ellipsoid
[2.90, 1, 0.30].

We modeled the deformation path using Flinn's (1978) matrix technique to separate compaction and tectonic strain. Other approaches are discussed by Oertel (1970), Sanderson (1976), Bell (1985), Wheeler (1986), Evans et al. (1989) and Oertel et al. (1989).

Not reporting the large volume reduction during compaction makes it difficult to visualize the strains involved in producing a slate. The constant volume convention to represent strain can seriously underestimate the amount of tectonic strain. For example, Wood & Oertel's (1980) estimate of tectonic thickening of beds in the Welsh slate belt was based on the constant volume strain of 're-

duction' spots. This corresponds to the distance, I, in Fig. 9 and includes the effect of compaction strain; whereas the strictly tectonic thickening corresponds to the distance, II.

SUMMARY AND CONCLUSIONS

Three complementary techniques were used to describe the fabric of kaolinite which was consolidated experimentally from slurries. Pole figures measured with the X-ray pole figure goniometer provide the most reliable quantitative description of preferred orientation; however, two methods of analyzing SEM micrographs also provide quantitative estimates. The preferred orientation of clay platelets correlates with strain, not stress, and is described by the March–Owens model, when one takes into account loss of volume. The platelets rotated towards the plane of flattening. The 'initial' porosities were slightly higher for dispersed than for flocculated slurries.

The preferred orientation of platy minerals in compacting clays and shales is a simple function of 'initial' and final porosities. In slates the volume change recorded by the preferred orientation includes the 'lost' porosity, which is nearly identical with the 'initial' porosity. Reasonable estimates of 'initial' porosities of clays and fine silts are in the range of 0.60–0.80 and are a function of grain size and mineralogy. Because volume reduction is such a large effect in pelitic rocks, we recommend separating compaction strain and tectonic strain and reporting four sets of strains or stretches rather than one. Errors associated with estimating the loss of volume and 'initial' porosity are certainly less than ignoring the effects of compaction strain on the fabric and strain ellipsoid.

In the relatively simple geologic situation of the Welsh slate belt—a linear fold belt with vertical slaty cleavage—a deformation path of uniaxial vertical compaction, gentle tilting of the beds, dewatering with uniaxial horizontal shortening followed by plane strain, is adequate to explain the gross features of the strain pattern and to simulate observed relationships at least in one locality. It also provides a reason why strain determination of 'reduction' spots tend to plot close to the contour for initial porosity, as noted, but not explained by Ramsay & Wood (1973).

REFERENCES

Abdelhamid, M. S. & Krizek, R. J. 1976. At-rest lateral earth pressure of a consolidating clay. *J. Geotech. Engng Div. ASCE* **102**, 721–738.

Altschaeffl, A. G. & Thevanayagam, S. 1991. Characterization of clay fabric. In: *Microstructure of Fine-grained Sediments* (edited by Bennett, R. H., Bryant, W. R. & Hulbert, M. H.). Springer, New York, 291–295.

Bachman, R. T. 1979. Acoustic anisotropy in marine sediments and sedimentary rocks. *J. geophys. Res.* **84**, 7661–7663.

Baker, D. W. & Carter, N. L. 1972. Seismic velocity anisotropy calculated for ultramafic minerals and aggregates. In: *Flow and Fracture of Rocks* (edited by Heard, H. C., Borg, I. Y., Carter, N. L. & Raleigh, C. B.). *Am. Geophys. Un. Geophys. Monogr.* **16**, 157–166.

Baker, D. W. & Wenk, H.-R. 1972. Preferred orientation in a low-symmetry quartz mylonite. *J. Geol.* **80**, 81–105.

Baker, D. W., Wenk, H. R. & Christie, J. M. 1969. X-ray analysis of preferred orientation in fine-grained quartz aggregates. *J. Geol.* **77**, 144–172.

Bell, A. 1985. Strain paths during slaty cleavage formation—the role of volume loss. *J. Struct. Geol.* **7**, 563–568.

Bennett, R. H., Bryant, W. R. & Keller, G. H. 1977. Clay fabric and geotechnical properties of selected submarine sediment cores from the Mississippi Delta. *NOAA Prof. Pap.* **9**, 1–86.

Bennett, R. H., Bryant, W. R. & Keller, G. H. 1981. Clay fabric of selected submarine sediments: Fundamental properties and models. *J. sedim. Petrol.* **51**, 217–232.

Bennett, R. H., O'Brien, N. R. & Hulbert, M. H. 1991. Determinants of clay and shale microfabric signatures: processes and mechanisms. In: *Microstructure of Fine-grained Sediments* (edited by Bennett, R. H., Bryant, W. R. & Hulbert, M. H.) Springer, New York, 5–32.

Bryant, W. R., Bennett, R. H. & Katherman, C. E. 1981. Shear strength, consolidation, porosity, and permeability of oceanic sediments. In: *The Sea, 7: The Oceanic Lithosphere* (edited by Emiliani, C.). Wiley, New York, 1555–1616.

Chawla, K. S. 1973. Effect of fabric on creep response of kaolinite clay. Unpublished Ph.D. dissertation, Northwestern University, Evanston, Illinois.

Crespi, J. M. 1986. Some guidelines for the practical application of Fry's method of strain analysis. *J. Struct. Geol.* **8**, 799–808.

Curtis, C. D., Lipshie, S. R., Oertel, G. & Pearson, M. J. 1980. Clay orientation in some Upper Carboniferous mudrocks, its relationship to quartz content and some inferences about fissility, porosity and compactional history. *Sedimentology* **27**, 333–339.

Dalziel, I. W. D. 1969. Pre-Permian history of the British Isles—A summary. In: *North Atlantic Geology and Continental Drift* (edited by Kay, M.). *Mem. Am. Ass. Petrol. Geol.* **12**, 5–31.

Dewey, J. F. 1969. Structure and sequence in paratectonic British Caledonides. In: *North Atlantic Geology and Continental Drift* (edited by Kay, M.). *Mem. Am. Ass. Petrol. Geol.* **12**, 309–335.

Edil, T. B. 1973. Influence of fabric and soil water potential on stress–strain response of clay. Unpublished Ph.D. dissertation, Northwestern University, Evanston, Illinois.

Edil, T. B. & Krizek, R. J. 1976. Influence of fabric and soil suction on the mechanical behavior of a kaolinitic clay. *Geoderma* **15**, 323–341.

Edil, T. B. & Krizek, R. J. 1977. Preparation of isotropically consolidated clay samples with random fabrics. *J. Testing & Eval.* **5**, 406–412.

Erslev, E. A. 1988. Normalized center-to-center strain analysis of packed aggregates. *J. Struct. Geol.* **10**, 201–209.

Erslev, E. A. & Ge, H. 1990. Least-squares center-to-center and mean object ellipse fabric analysis. *J. Struct. Geol.* **12**, 1047–1059.

Evans, K. F., Oertel, G. & Engelder, T. 1989. Appalachian stress study 2. Analysis of Devonian shale core: some implications for the nature of contemporary stress variations and Alleghanian deformation in Devonian rocks. *J. geophys. Res.* **94**, 7155–7170.

Faust, L. Y. 1951. Seismic velocity as a function of depth and geologic time. *Geophysics* **16**, 192–206.

Feeser, V. 1986. Entwicklung eines Verfahrens zur Bestimmung der geologischen Vorbelastung von Tonen auf gefügekundlicher Grundlage. *Geol. Jb. Reihe C* **46**, 3–136.

Flinn, D. 1978. Construction and computation of three-dimensional progressive deformations. *J. geol. Soc. Lond.* **135**, 291–305.

Fry, N. 1979. Random point distributions and strain measurement in rocks. *Tectonophysics* **60**, 89–105.

Griffiths, F. J. & Joshi, R. C. 1990. Clay fabric response to consolidation. *Appl. Clay Sci.* **5**, 37–66.

Hamilton, E. L. & Bachman, R. T. 1982. Sound velocity and related properties of marine sediments. *J. acoust. Soc. Am.* **72**, 1891–1904.

Heard, H. C. & Lin, W. 1986. High-pressure mechanical and sonic properties of a Devonian shale from West Virginia. Unconventional Gas Program. Lawrence Livermore National Laboratory, Rep. UCID-20612, NTIS. 1–41.

Jones, L. E. A. & Wang, H. F. 1981. Ultrasonic velocities in Cretaceous shales from the Williston basin. *Geophysics* **46**, 288–297.

Kanatani, K.-I. 1984. Stereological determination of structural anisotropy. *Int. J. Engng Sci.* **22**, 531–546.

Kanatani, K.-I. 1985. Procedures for sterological estimation of structural anisotropy. *Int. J. Engng Sci.* **23**, 587–598.

Krizek, R. J., Chawla, K. S. & Edil, T. B. 1977. Directional creep response of anisotropic clays. *Géotechnique* **27**, 37–51.

Krizek, R. J., Edil, T. B. & Ozaydin, I. K. 1975. Preparation and identification of clay samples with controlled fabric. *Engng Geol.* **9**, 13–38.

Magara, K. 1978. *Compaction and Fluid Migration.* Elsevier, Amsterdam.

March, A. 1932. Mathematische Theorie der Regelung nach der Korngestalt bei affiner Deformation. *Z. Kristallogr.* **81**, 285–297.

Mardia, K. V. 1972. *Statistics of Directional Data.* Academic Press, London, 233–234, 253–254.

Martin, R. T. 1965. Quantitative fabric of consolidated kaolinite. Research in Earth Physics, Phase Rep. No. 4 to U.S. Army Waterways Experiment Station, Corps of Engineers, Vicksburg, Mississippi, Rep. R65-47.

Martin, R. T. 1966. Quantitative fabric of wet kaolinite. *Clays Clay Miner.* **14**, 271–287.

Martin, R. T. & Ladd, C. C. 1975. Fabric of consolidated kaolinite. *Clays Clay Miner.* **23**, 17–25.

McConnachie, I. 1974. Fabric changes in consolidated kaolin. *Géotechnique* **24**, 207–222.

Meade, R. H. 1966. Factors influencing the early stages of the compaction of clays and sands—review. *J. Sedim. Petrol.* **36**, 1085–1101.

Mitchell, J. K. 1976. *Fundamentals of Soil Behavior.* Wiley, New York.

Monté, J. L. & Krizek, R. J. 1976. One-dimensional mathematical model for large-strain consolidation. *Géotechnique* **26**, 495–510.

Morgenstern, N. R. & Tchalenko, J. S. 1967. The optical determination of preferred orientation in clays and its application to the study of microsctructures in consolidated kaolin. *Proc. R. Soc. Lond.* **A300**, 218–250.

Nye, J. F. 1957. *Physical Properties of Crystals.* Clarendon Press, Oxford.

Oertel, G. 1970. Deformation of a slaty, lapillar tuff in the Lake District, England. *Bull. geol. Soc. Am.* **81**, 1173–1188.

Oertel, G. 1983. The relationship of strain and preferred orientation of phyllosilicate grains in rocks—a review. *Tectonophysics* **100**, 413–447.

Oertel, G. & Curtis, C. D. 1972. Clay–ironstone concretion preserving

fabrics due to progressive compaction. *Bull. geol. Soc. Am.* **83**, 2597–2606.

Oertel, G., Engelder, T. & Evans, K. 1989. A comparison of the strain of crinoid columnals with that of their enclosing silty and shaly matrix on the Appalachian Plateau, New York. *J. Struct. Geol.* **11**, 975–993.

Owens, W. H. 1973. Strain modification of angular density distributions. *Tectonophysics* **16**, 249–261.

Ramsay, J. G. 1967. *Folding and Fracturing of Rocks.* McGraw-Hill, New York.

Ramsay, J. G. & Huber, M. I. 1983. *The Techniques of Modern Structural Geology, Volume 1: Strain Analysis.* Academic Press, New York.

Ramsay, J. G. & Wood, D. S. 1973. The geometric effects of volume change during deformation processes. *Tectonophysics* **16**, 263–277.

Rieke, H. H. & Chilingarian, G. V. 1974. *Compaction of Argillaceous Sediments.* Elsevier, Amsterdam, 1–351.

Sanderson, D. J. 1976. The superposition of compaction and plane strain. *Tectonophysics* **30**, 35–54.

Schiller, H. J. 1980. Röntgenographische Texturuntersuchungen an feinkörningen Sedimenten unterschiedlischer Kompaktion. *Bochumer geol. geotech. Arb.* **4**.

Sheeran, D. E. & Krizek, R. J. 1971. Preparation of homogeneous soil samples by slurry consolidation. *J. Mater.* **6**, 356–373.

Tullis, T. E. 1971. Experimental development of preferred orientation of mica during recrystallization. Unpublished Ph.D. dissertation, University of California, Los Angeles.

Tullis, T. E. 1976. Experiments on the origin of slaty cleavage and schistosity. *Bull. geol. Soc. Am.* **87**, 745–753.

Tullis, T. E. & Wood, D. S. 1975. Correlation of finite strain from both reduction bodies and preferred orientation of mica in slate from Wales. *Bull. geol. Soc. Am.* **86**, 632–638.

Watson, G. S. 1965. Equatorial distributions on a sphere. *Biometrika* **52**, 193–201.

Watson, G. S. 1966. The statistics of orientation data. *J. Geol.* **74**, 786–797.

Watson, G. S. 1983. *Statistics on Spheres.* J. Wiley & Sons, New York.

Wheeler, J. 1986. Strain analysis in rocks with pretectonic fabrics. *J. Struct. Geol.* **8**, 887–896.

Wood, D. S. 1974. Current view of the development of slaty cleavage. *Annu. Rev. Earth Planet. Sci.* **2**, 369–401.

Wood, D. S. & Oertel, G. 1980. Deformation in the Cambrian slate belt of Wales. *J. Geol.* **88**, 285–308.

Wood, D. S., Oertel, G., Singh, J. & Bennett, H. F. 1976. Strain and anisotropy in rocks. *Philos. Trans. R. Soc. London.* **283**, 27–42.

Yong, R. N. & Warkentin, B. P. 1975. *Soil Properties and Behavior.* Elsevier, Amsterdam.